

Measurement of solid-state optical refrigeration by two-band differential luminescence thermometry

W. M. Patterson,^{1,*} D. V. Seletskiy,¹ M. Sheik-Bahae,¹ R. I. Epstein,² and M. P. Hehlen²

¹The University of New Mexico, 800 Yale Boulevard Northeast, Albuquerque, New Mexico 87131, USA

²Los Alamos National Laboratory, Los Alamos, New Mexico 87545, USA

*Corresponding author: wendy5@unm.edu

Received October 20, 2009; revised December 14, 2009; accepted January 5, 2010;
posted January 5, 2010 (Doc. ID 118794); published February 26, 2010

We present a non-contact optical technique for the measurement of laser-induced temperature changes in solids. Two-band differential luminescence thermometry (TBDLT) achieves a sensitivity of ~ 7 mK and enables a precise measurement of the net quantum efficiency of optical refrigerator materials. The TBDLT detects internal temperature changes by decoupling surface and bulk heating effects via time-resolved luminescence spectroscopy. Several Yb³⁺-doped fluorozirconate (ZrF₄-BaF₂-LaF₃-AlF₃-NaF-InF₃, ZBLANI) glasses fabricated from precursors of varying purity and by different processes are analyzed in detail. A net quantum efficiency of $(97.39 \pm 0.01)\%$ at 238 K (at a pump wavelength of 1020.5 nm) is found for a ZBLANI:1% Yb³⁺ laser-cooling sample produced from metal fluoride precursors that were purified by chelate-assisted solvent extraction and dried in hydrofluoric gas. In comparison, a ZBLANI:1% Yb³⁺ sample produced from commercial-grade metal fluoride precursors showed pronounced laser-induced heating that is indicative of a substantially higher impurity concentration. The TBDLT enables rapid and sensitive benchmarking of laser-cooling materials and provides critical feedback to the development and optimization of high-performance optical cryocooler materials. © 2010 Optical Society of America

OCIS codes: 160.5690, 300.2530, 300.6430.

1. INTRODUCTION

The first successful laser-induced cooling of a solid in 1995 produced a mere 0.3 K of cooling in the Yb³⁺-doped fluorozirconate glass (ZrF₄-BaF₂-LaF₃-AlF₃-NaF, ZBLAN) [1]. Since then, the field has made a steady progress in material preparation methods [2,3], optical configurations [4], and characterization techniques; and this effort has recently resulted in the laser cooling of a LiYF₄:Yb³⁺ bulk crystal to 164 K [5]. This temperature rivals high-end thermoelectric coolers [6] and underscores the potential of laser cooling as an emerging solid-state cryogenic refrigeration technology. Laser cooling down to ~ 70 K is theoretically possible in Yb³⁺-doped materials [7,8], and even lower temperatures may be achieved with other rare-earth ions (such as Tm³⁺ or Dy³⁺) that have smaller energy gaps and higher laser-cooling efficiencies.

The ability to accurately and rapidly measure the laser-cooling efficiency of a sample is critical for the systematic development of the purification and fabrication processes associated with the preparation of optical refrigerator materials. The measurement of the laser-cooling efficiency, however, is met with difficulties. Significant pump light absorption and a corresponding significant temperature change are only achieved in multi-pass pump geometries. These involve not only the setup and alignment of a pump cavity, but also the laborious preparation of a sample with high quality optical surfaces. Furthermore, non-contact thermometry is required since a temperature sensor in thermal contact with the sample would potentially become a heat load when exposed to the pump light and sample luminescence. A simple single-pass pump geometry and a thermometry method that is insensitive to the

surface preparation would greatly facilitate the sample characterization and enable expeditious feedback of laser-cooling performance data to the material development effort. A non-contact thermometry method is therefore needed that (1) has sufficiently high sensitivity to detect the <0.1 K temperature changes that are typical of single-pass pumping of laser-cooling materials, (2) is insensitive to laser-induced heating at imperfect sample surfaces, (3) can be used at low temperatures, and (4) can resolve the fast thermal response in the time domain. Luminescence spectra have been used in the past as non-contact internal temperature probes and, in the case of rare-earth-doped materials, absolute temperature measurements with $\pm 0.1^\circ\text{C}$ accuracy have been reported [9]. The changes in the luminescence intensity distribution for rare-earths are quite subtle, especially when compared to those observed in semiconductors where substantial wavelength shifts produce large changes in the intensity distribution [10]. In contrast, the $4f$ electrons in rare-earths are well shielded from the environment in the solid, and crystal field transitions therefore do not appreciably shift with temperature. The temperature-induced intensity changes in rare-earth luminescence spectra are thus primarily due to changes in (1) the Boltzmann population of the crystal field levels of the emitting state and (2) the homogeneous linewidths of the individual crystal field transitions. Seletskiy *et al.* reported a time-resolved technique that detects small laser-induced temperature changes inside the sample via changes in its luminescence spectrum [11]. Their differential luminescence thermometry (DLT) experiment correlated the relative intensity change of two adjacent regions in the luminescence

Report Documentation Page

Form Approved
OMB No. 0704-0188

Public reporting burden for the collection of information is estimated to average 1 hour per response, including the time for reviewing instructions, searching existing data sources, gathering and maintaining the data needed, and completing and reviewing the collection of information. Send comments regarding this burden estimate or any other aspect of this collection of information, including suggestions for reducing this burden, to Washington Headquarters Services, Directorate for Information Operations and Reports, 1215 Jefferson Davis Highway, Suite 1204, Arlington VA 22202-4302. Respondents should be aware that notwithstanding any other provision of law, no person shall be subject to a penalty for failing to comply with a collection of information if it does not display a currently valid OMB control number.

1. REPORT DATE 26 FEB 2010		2. REPORT TYPE		3. DATES COVERED 00-00-2010 to 00-00-2010	
4. TITLE AND SUBTITLE Measurement of solid-state optical refrigeration by two-band differential luminescence thermometry				5a. CONTRACT NUMBER	
				5b. GRANT NUMBER	
				5c. PROGRAM ELEMENT NUMBER	
6. AUTHOR(S)				5d. PROJECT NUMBER	
				5e. TASK NUMBER	
				5f. WORK UNIT NUMBER	
7. PERFORMING ORGANIZATION NAME(S) AND ADDRESS(ES) University of New Mexcio,800 Yale Boulevard Northeast,Albuquerque,NM,87131				8. PERFORMING ORGANIZATION REPORT NUMBER	
9. SPONSORING/MONITORING AGENCY NAME(S) AND ADDRESS(ES)				10. SPONSOR/MONITOR'S ACRONYM(S)	
				11. SPONSOR/MONITOR'S REPORT NUMBER(S)	
12. DISTRIBUTION/AVAILABILITY STATEMENT Approved for public release; distribution unlimited					
13. SUPPLEMENTARY NOTES					
14. ABSTRACT					
15. SUBJECT TERMS					
16. SECURITY CLASSIFICATION OF:			17. LIMITATION OF ABSTRACT	18. NUMBER OF PAGES	19a. NAME OF RESPONSIBLE PERSON
a. REPORT unclassified	b. ABSTRACT unclassified	c. THIS PAGE unclassified			

spectrum to a temperature change and, using a monochromator in conjunction with a balanced pair of photodiodes, achieved millikelvin sensitivity for a GaAs heterostructure sample.

In this paper we present a two-band differential luminescence thermometry (TBDLT) method that achieves ~ 7 mK sensitivity in rare-earth-doped materials. By selecting two bands in the luminescence spectrum by interference filters, in combination with large core optical fibers and highly amplified balanced photodetectors, an improved optical throughput and significantly higher sensitivity are achieved compared to earlier DLT studies [9]. The TBDLT method offers substantially higher sensitivity than data acquisition (DAQ) with a commercial luminescence spectrometer and is a tool to study laser-induced thermal processes in any doped luminescent solid. In this study, we apply the TBDLT to rare-earth-doped optical refrigerator materials. We present a detailed analysis of several Yb^{3+} -doped fluorozirconate glasses and show that the measured laser-cooling performance correlates with the fabrication history of the sample, providing valuable information for further optimizing the material preparation processes. The TBDLT technique and data analysis methods are described in Section 2 followed by a description of the experiments in Section 3. Section 4 presents measurements of two ZBLAN:Yb $^{3+}$ laser-cooling samples, and Section 5 summarizes the findings of this study.

2. TBDLT

A. Principle of Operation

The TBDLT monitors the luminescence from a sample and deduces laser-induced temperature changes from changes in the spectral distribution. Laser-induced temperature changes can arise from (1) local cooling or heating inside the material and (2) heating at imperfect sample surfaces. The main advantage of the TBDLT is in its ability to distinguish the intrinsic laser-induced cooling or heating processes from laser-induced heating at the sample surfaces, thereby eliminating the need for a difficult and laborious surface preparation and thus greatly facilitating the sample characterization. Bulk cooling or heating is decoupled from surface heating by monitoring laser-induced temperature changes in the time domain and in a small internal volume. This can be achieved because internal cooling or heating processes dominate the temperature change immediately after turning on the laser, and it is only after some time that the heat generated at the sample surface reaches the locally monitored excitation volume inside the sample. The experiment, therefore, consists of turning on the laser for a period of time and monitoring the temperature change that occurs due to intrinsic cooling or heating processes, followed by turning off the laser for a period of time for the sample to thermalize back to the ambient temperature. This sequence is repeated, and the signals are averaged over many cycles. This cycled pumping method also eliminates the effects of long-term ambient temperature drifts. Such an experiment is also, importantly, insensitive to reabsorption effects which plague experiments taken with an infrared camera, for example.

Let us now look more closely at one such pumping cycle for the example of the Yb^{3+} -doped fluorozirconate glass ($\text{ZrF}_4\text{-BaF}_2\text{-LaF}_3\text{-AlF}_3\text{-NaF-InF}_3$, ZBLANI). Assume a bulk sample of ZBLANI:Yb $^{3+}$ in thermal equilibrium with the surrounding bath temperature. A pump laser with a Gaussian transverse intensity distribution is focused into the bulk of the sample and turned on at time $t=0$. A spatially non-uniform and time-dependent temperature distribution will develop as a result of laser-induced internal heating or cooling processes. As illustrated in Fig. 1, the ${}^2F_{5/2} \rightarrow {}^2F_{7/2}$ luminescence spectrum of Yb^{3+} is temperature dependent, and the Yb^{3+} ions can therefore serve as local temperature probes. Specifically, the ZBLANI:Yb $^{3+}$ luminescence spectrum contains four spectral regions in which the luminescence intensity either increases (regions A and C) or decreases (regions B and D) as the sample temperature is raised (see Fig. 1). We will focus on regions A and D since they can be easily selected with commercial bandpass filters (see Subsection 3.B). The Yb^{3+} luminescence spectral distribution $I(\lambda, T, t)$ at time t is determined by the local temperature T , and the respective differential luminescence signal is defined as [12]

$$\Xi(T, t) = \frac{I_A^*(T, t) - I_D^*(T, t)}{I_A^*(T, t) + I_D^*(T, t)}. \quad (1)$$

In Eq. (1), $I_A^*(T, t)$ and $I_D^*(T, t)$ are integrals over the product of the luminescence spectrum, $I(\lambda, T, t)$, and the bandpass filter transmission spectra $\theta_A(\lambda)$ and $\theta_D(\lambda)$, respectively, i.e.,

$$I_A^*(T, t) = \int I(\lambda, T, t) \theta_A(\lambda) d\lambda, \\ I_D^*(T, t) = \int I(\lambda, T, t) \theta_D(\lambda) d\lambda, \quad (2)$$

where Fig. 2 shows this overlap for our particular example.

Finally, since luminescence is collected from a finite volume, we must account for the temperature distribution

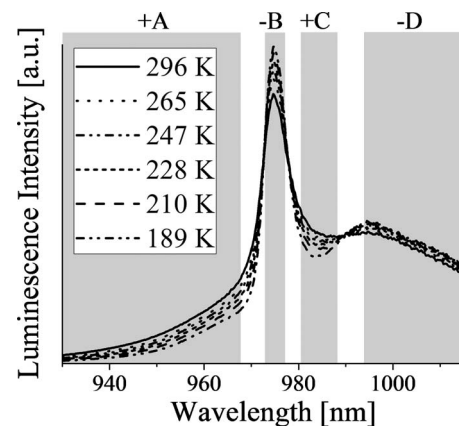


Fig. 1. Area normalized luminescence spectra at different temperatures for Sample 4 (see Table 1). As the temperature is increased, the luminescence intensity of regions A and C increases while the luminescence intensity of regions B and D decreases. Note that the full spectrum, which extends to >1030 nm, is not shown for clarity.

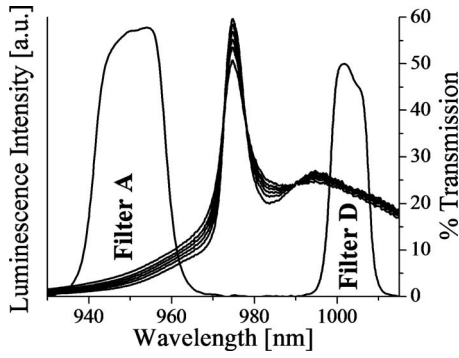


Fig. 2. Area normalized luminescence spectra at different temperatures for Sample 4 (left axis) and transmission spectra of the commercial bandpass filters (right axis) used in the TBDLT experiment. Filters A and D are chosen such as to select and integrate a sizable portion of the luminescence spectrum regions +A and -D (see Fig. 1), respectively.

in the collection volume not being uniform. The measured TBDLT signal $\Xi(T, t)$ is therefore obtained by the integration of Eq. (1) over the transversal plane. Note that the luminescence intensity is proportional to the excited state population $n_2(x, y, t)$, and $\Xi(T, t)$ is thus weighted by $n_2(x, y, t)$ accordingly, as discussed in detail elsewhere [12]. $\Xi(T, t)$ is defined such that it decreases with decreasing sample temperature, i.e., laser-induced cooling will cause the value of $\Xi(T, t)$ to decrease with time. The normalization to the total luminescence intensity $I_A^* + I_D^*$ accounts for the temperature dependence of the absorption coefficient as well as for drifts in the optical alignment and laser power. The change in $\Xi(T, t)$ is thus a direct measure for the laser-induced temperature change in the collection volume. $\Xi(T, t)$ can be found, in principle, from a series of luminescence spectra recorded in rapid succession after the laser has been turned on. The sensitivity of commercial luminescence spectrometers, however, was found to be insufficient and did not allow for sufficiently high DAQ rates to resolve $\Xi(T, t)$. This provided the main motivation for developing the TBDLT method presented here.

B. Data Analysis Method

The local temperature in the excited volume, and thus the measured TBDLT signal $\Xi(T, t)$, varies as a function of time after turning on the laser. $\Xi(T, t)$ therefore depends on several factors including (1) host material properties such as heat capacity, thermal conductivity, and the mass density; (2) pump beam characteristics such as beam waist and laser power; (3) the rare-earth dopant ion density and relaxation rate; (4) the net quantum efficiency η , which is affected by impurity concentrations; and (5) the sample size. A formal description of the spatial and temporal dependence of temperature in laser-cooling materials is given elsewhere [12]. From these calculations we expect the TBDLT signal $\Xi(T, t)$ to have three temporal components. There is an initial fast component with a time constant governed by the excited state lifetime of the rare-earth ion, and it is characteristic of how quickly heat is removed from (cooling) or deposited into (heating) the sample in the small excitation volume defined by the focused laser. A subsequent second slow component has a

time constant that is governed by the material properties, and it is characteristic of how quickly heat flows out of (cooling) or into (heating) the much larger bulk volume of the sample. Finally, the sample reaches thermal equilibrium and $\Xi(T, t)$ reaches a steady-state value. The period of time required for the steady state to develop depends on the sample size and was found to be >5 s for the samples of this study. The experimental setup, described in detail in Subsection 3.B, did not allow for measurement of the initial fast component and therefore only captured the second slow component (beginning at $t \approx 25$ ms in ZBLANI:Yb³⁺). The functional form of the slow component of the $\Xi(T, t)$ transient follows a simple power law [12],

$$\Xi(T, t) \propto t^\vartheta. \quad (3)$$

The slope ϑ of the respective line in the double-logarithmic representation is a metric for the laser-induced temperature change, and it can be used as a characteristic TBDLT parameter that provides a measure of the laser-cooling performance of the material at a given bath temperature. Laser-induced cooling or heating is therefore present if $\vartheta < 0$ or $\vartheta > 0$, respectively. $\vartheta = 0$ corresponds to the temperature at which the rates of laser-induced heating and cooling processes are exactly balanced. As shown in the next section, this heat-balanced point is of particular significance as it can be used to determine the net quantum efficiency of the material.

C. TBDLT of Optical Refrigerator Materials

In rare-earth-doped optical refrigerators, a pump laser is tuned to excite the rare-earth ion at a wavelength λ_p that is longer than the mean luminescence wavelength ($\bar{\lambda}_f$), and the thermal energy is subsequently removed from the solid by the anti-Stokes luminescence. The laser-cooling process is characterized by the cooling efficiency

$$\eta_{\text{cool}} = (\eta\lambda_p - \bar{\lambda}_f)/\bar{\lambda}_f, \quad (4)$$

where η is the net quantum efficiency of the rare-earth excited state [13]. η is defined as

$$\eta(\lambda_p, T) = \eta_{\text{abs}}\eta_{\text{ext}}, \quad (5)$$

where η_{ext} describes the efficiency with which an excited ion produces a luminescence photon that escapes from the sample. The absorption efficiency $\eta_{\text{abs}} = \alpha_r(\lambda)/(\alpha_r(\lambda) + \alpha_b)$ accounts for the fraction of excited photons that are engaged in cooling, where $\alpha_r(\lambda)$ is the resonant (e.g., Yb³⁺) absorption at a given wavelength and α_b is the background absorption of the material, typically assumed to be independent of the pump wavelength and temperature. Note that η is a function of both temperature and pump wavelength, largely through the absorption term η_{abs} , but also due to the spectral overlap between the rare-earth ion emission and the impurity absorption. Previous studies have identified certain transition metal ions (e.g., Cu²⁺, Fe²⁺, Co²⁺, and Ni²⁺) and impurities having high-energy vibrational modes (e.g., OH⁻ and H₂O) as contributors to lowering the net quantum efficiency [14]. It was estimated that the concentration of such impurities must be below the 100 ppb range for a material to realize practical cooling efficiencies at cryogenic tempera-

tures [14]. The measurement of impurity concentrations is therefore a prerequisite for the systematic development of advanced purification and fabrication methods for laser-cooling materials.

Here we use the net quantum efficiency of the material as an indirect measure of the aggregate impurity concentration, providing a quantitative benchmark for the quality of a sample. While measurements of absolute quantum efficiencies of luminescent materials are notoriously difficult, particularly when η is close to 1, the situation is fortunate in laser-cooling materials. Here, the wavelength difference $\eta\lambda_p - \bar{\lambda}_f$ can be tuned to one of the two points where laser-induced cooling and heating are exactly balanced and no laser-induced temperature change occurs. Figure 3 illustrates the normalized laser-induced change in temperature ΔT (which is proportional to η_{cool}) as a function of the pump wavelength. The heat-balanced points (solid dots) can be reached by tuning $\eta\lambda_p - \bar{\lambda}_f$ either by (1) changing λ_p at a fixed sample temperature and observing the wavelength where this crossover point occurs (referred to as the zero-crossing wavelength λ_{ZCW}) or (2) changing $\bar{\lambda}_f(T)$ via the sample temperature at a fixed laser wavelength. In the latter case, ϑ then gradually increases as the sample temperature is lowered (and $\eta\lambda_p - \bar{\lambda}_f$ is decreased via increasing $\bar{\lambda}_f$) until laser-induced cooling switches over to laser-induced heating ($\vartheta > 0$) at a characteristic sample temperature. This crossover point is referred to as the zero-crossing temperature (T_{ZCT}) where laser-induced cooling and heating are exactly balanced, i.e., $\vartheta = 0$. This is the lowest temperature at which the sample can sustain laser-induced cooling and is yet another benchmark for laser-cooling performance. At the two heat-balanced points, the laser-induced temperature change $\Delta T \propto \eta_{cool} = (\eta\lambda_p - \bar{\lambda}_f)/\bar{\lambda}_f = 0$ and the net quantum efficiency $\eta(\lambda_p, T) = \bar{\lambda}_f/\lambda_p$ can be calculated from two easily

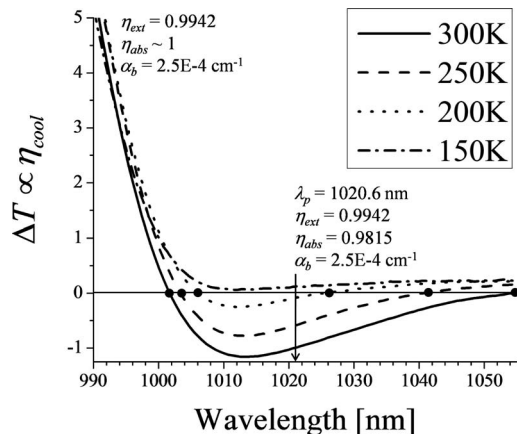


Fig. 3. Calculation of the normalized laser-induced temperature change as a function of wavelength illustrating the two points for a given sample temperature where ΔT (and thus η_{cool}) goes to zero. The long-wavelength zero crossing arises due to $\alpha_b > 0$. A widely tunable pump source would clearly be required to predict T_{ZCT} for this long-wavelength zero crossing. However, near this zero crossing, a large ΔT is observed, allowing greater sensitivity. The short-wavelength zero crossing occurs when $\lambda_p = \bar{\lambda}_f$. Here, α_r is large and α_b can be neglected, allowing for a measurement of η_{ext} . The values of η_{ext} , η_{abs} , and α_b used for this example calculation are also shown.

observable quantities. Laser-induced temperature changes near the heat-balanced point are small, and a sensitive non-contact thermometry method is therefore needed.

Changing the pump wavelength to locate one of the temperature balanced points is a conceivably easier experiment; however, widely tunable high power lasers are not necessarily available at the desired pump wavelengths. At longer pump wavelengths, we can take advantage of the second approach to finding a temperature balanced point when such tunable pump sources are not readily available, as was the case for our particular experiment. At shorter wavelengths, where $\lambda_p \approx \bar{\lambda}_f$, α_b is insignificant with respect to the large α_r . Therefore, $\eta_{abs} \sim 1$ and thus $\eta \sim \eta_{ext}$ and the cooling efficiency should be approximately linear with respect to λ_p . In this case, η_{ext} can be measured by a standard fractional heating experiment [14] that observes ΔT as a function of λ_p to find λ_{ZCW} . However, in the longer-wavelength region, α_r is significantly smaller, and α_b becomes more significant and must be accounted for. Assuming that η_{ext} does not vary with the wavelength, α_r can be found at the shorter wavelength and used to determine η_{abs} [in Eq. (5)]. Additionally, given $\alpha_r(T)$, we can estimate the background absorption α_b . Thus, each zero-crossing point provides valuable information on η_{ext} and α_b and thus on the impurity concentration.

An experiment thus consists of measuring $\Xi(T, t)$ transients at different sample temperatures, fitting the power law [Eq. (3)] to the slow component of each transient, calculating the slopes ϑ , deducing T_{ZCT} from a plot of ϑ versus the sample temperature, and calculating $\eta = \bar{\lambda}_f/\lambda_p$ from $\bar{\lambda}_f$ at T_{ZCT} . The measured net quantum efficiency η or T_{ZCT} can be used as a measure for the quality of a laser-cooling sample, where a higher value of η or lower T_{ZCT} is indicative of a sample with a lower level of impurities. This method enables performance benchmarking of laser-cooling samples by correlating lower impurity samples with lower T_{ZCT} values.

3. EXPERIMENTAL SECTION

A. Yb³⁺-Doped Fluorozirconate Glasses

Several Yb³⁺-doped ZBLANI glasses were characterized by the TBDLT method described in Section 2. Table 1 summarizes the glass compositions and provides comments on sample preparation conditions. Sample 1 was synthesized from commercially available high-purity metal fluoride precursors without conducting any further purification except the mandatory drying and fluorination of metal fluoride precursors in hot hydrogen fluoride gas. Samples 2–4 incorporate progressive stages of the solvent-extraction purification currently under development in our laboratory, a process that aims at reducing transition-metal impurities to low-parts-per-billion levels [2,3]. Samples 5 and 6 are identical to Sample 4, except for a higher 2 mol. % Yb³⁺ concentration in Sample 5 and sublimated (another purification technique) rather than solvent-extracted ZrF₄ in Sample 6. Sample 7 is a commercial ZBLAN:Yb³⁺ sample procured from IPG Photon-

Table 1. Yb³⁺-Doped Fluorozirconate Glass Samples Used in This Study. The ZBLANI Composition is Given in Mole Percent of the Respective ZBLANI Metal Fluoride Constituents. A Detailed Description of Solvent-Extraction and Hydrogen Fluoride Gas Drying Processes is Given in [2]

Sample Number	Yb ³⁺ (mol. %)	ZBLANI Composition (mol. %)	Sample Descriptions and Preparation Notes
1	1	54–21–3.5–3.5–16.5–0.5	Synthesized from commercial metal fluoride precursors without further purification. Some bulk scattering.
2	1	54–21–3.5–3.5–16–1	First generation solvent-extraction purification process. Some bulk scattering.
3	1	53–20–3–3–17.5–2.5	Second generation solvent-extraction purification process. Excellent optical quality.
4	1	53–20–3–3–17.5–2.5	Third generation solvent-extraction purification process. Improved hydrogen fluoride gas drying process. Excellent optical quality.
5	2	53–20–2–3–17.5–2.5	Same as Sample 4 but with 2% Yb ³⁺ doping.
6	1	53–20–3–3–17.5–2.5	Same as Sample 4 but ZrF ₄ was purified by sublimation rather than solvent extraction.
7	2	Unknown	Commercial ZBLAN sample from IPG Photonics.

ics that has shown good laser-cooling performance, and it was used as a point of reference in this study.

B. TBDLT Experiments

The TBDLT experimental setup is shown schematically in Fig. 4. The sample was mounted on the temperature-controlled cold finger of a liquid-nitrogen flow cryostat (Helitran, LT-3-110) and cooled to the desired temperature in the 100–300 K range. The ambient sample temperature was measured by a miniature (1.5 mm diameter) calibrated silicon diode (Lakeshore DT-421) mounted directly onto the surface of the sample using a small amount of Apiezon grease. Direct measurement of the sample temperature was important because different samples exhibited different temperature gradients between the sample and the cold finger temperature sensor depending on the quality of the thermal contact. The TBDLT decouples laser-induced temperature changes at the surface from those inside the sample in the time domain, and we confirmed that any potential heating of the small silicon diode at the sample surface during exposure to laser and luminescence light did not affect the measurement.

A diode-pumped continuous-wave (CW) Yb:yttrium aluminum garnet laser (Nanolase, DP12011-T01) equipped with a tunable birefringent filter (1010–1050 nm) produced ~3.5 W of pump power at 1020.5 nm with a Gaussian intensity distribution. This pump wavelength was chosen as a compromise between maximizing the absorbed power for the entire temperature range (favoring a shorter wavelength) and maximizing the laser-cooling efficiency (favoring a longer wavelength). The excitation of the sample was performed in a time sequence consisting of pump laser exposure for 5 s during which the sample heated or cooled, followed by the pump laser being off for 5 s during which the sample equilibrated back to the ambient temperature set by the cryostat. A function genera-

tor was used to control the respective laser shutter and to trigger the DAQ system. The time constant of the mechanical laser shutter was ~20 ms, and the luminescence transient data collected for $t < 25$ ms were therefore discarded. The pump beam was focused into the sample and, in order to reduce the effects of luminescence reabsorption, the focal spot was aligned near the sample surface through which the luminescence was collected.

The sample luminescence was collected and collimated by a 2 in. diameter lens ($f=60$ mm) and coupled into a 600 μm diameter multimode fiber by a second lens ($f=100$ mm). For reference, the luminescence spectrum was recorded with an Ocean Optics mini-spectrometer (SD2000) at each sample temperature. The luminescence emerging from the multimode fiber was collimated and then divided into two beams by a 50:50 non-polarizing

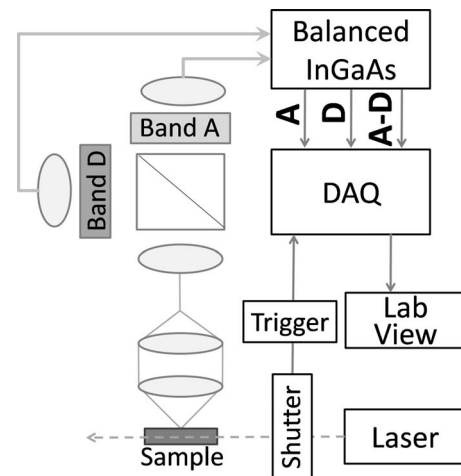


Fig. 4. Schematic of the TBDLT experimental setup described in detail in Subsection 3.B. The transmission spectra of the filters used to define bands A and D are shown in Fig. 2.

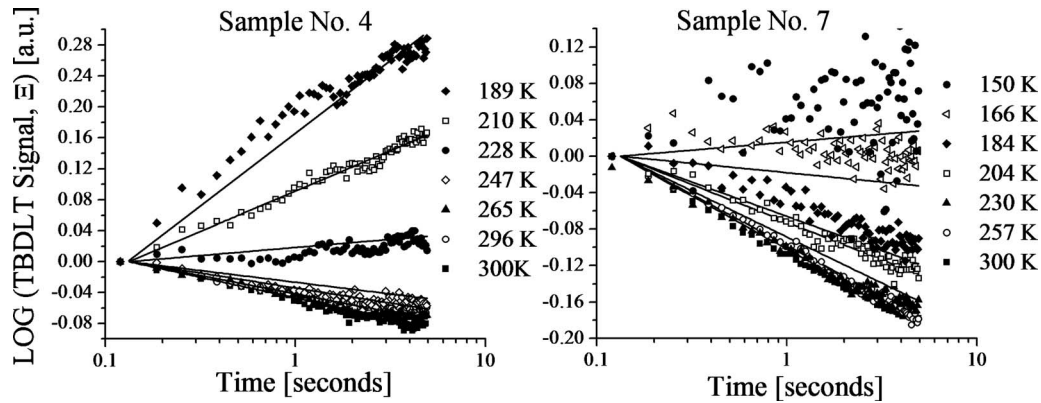


Fig. 5. Transient TBDLT signal corresponding to the laser-induced temperature change at different ambient sample temperatures for Samples 4 (left) and 7 (right). Negative slopes indicate laser-induced cooling while positive slopes indicate laser-induced heating. The solid lines are fits of the power law [Eq. (3)] to the experimental data.

beam splitter cube. One beam was filtered by bandpass filter A (Andover Corporation, 950FS10), and the other beam was filtered by bandpass filter D (Andover Corporation, 100FS10). Figure 2 shows the transmission spectra of the commercial interference filters used to select bands A and D of the Yb^{3+} luminescence spectrum. Note that the spectrally narrower bands B and C (indicated in Fig. 1) were omitted for simplicity and because they could not be selected easily with commercially available bandpass filters. Each filtered beam was re-coupled into respective 600 μm diameter multimode fibers that terminated on a pair of InGaAs balanced photodiodes (ThorLabs PDB150C). The PDB150C balanced photodetector consists of two photodiodes with well matched responsivities and provides separate voltage outputs that are proportional to the optical power received in each of bands A and D. In addition, the PDB150C includes an ultra-low noise high speed transimpedance amplifier that generates an output voltage proportional to the *difference* in the optical power in bands A and D, i.e., $(I_A^* - I_D^*)$. The voltage at each of these three detector outputs was independently and simultaneously measured by a multi-channel DAQ board (Measurement Computing, USB-1616FS) that provided 16 bit resolution at a simultaneous acquisition rate of 36 kHz/channel, enabling time resolutions of up to $\sim 30 \mu\text{s}$ in the measured TBDLT transients. The DAQ board transferred the data via universal serial bus to a personal-computer-based LabView application that captured and analyzed the data in real time. To achieve the maximum dynamic range, the two filtered beam paths were aligned for each measurement such that the measured difference signal $(I_A^* - I_D^*)$ was zero for the CW pumping.

The transients recorded during each 5 s pump interval were averaged until the desired signal-to-noise ratio in the TBDLT transient was obtained. Typical averaging times ranged from 10 min (60 intervals) to 2 h (720 intervals), depending on the luminescence intensity available at a particular temperature.

4. RESULTS AND DISCUSSION

The TBDLT characterization included six Yb^{3+} -doped ZBLANI samples prepared in our laboratory (Samples 1–6) and a commercial 2% Yb^{3+} -doped ZBLAN sample

(IPG Photonics; Sample 7) which had shown substantial laser cooling in earlier experiments (see Table 1). Figure 5 shows TBDLT transients for Samples 4 and 7 at different temperatures. The solid lines represent least-squares fits of the power law in Eq. (3) to the transient data. The measured TBDLT transients are described well by this functional shape. Both samples exhibit laser cooling at 300 K as evident from the negative slope of the transient at that temperature. The magnitude of cooling gradually diminishes as the temperature is lowered, i.e., as $\eta\lambda_p - \bar{\lambda}_f$ decreases due to the increase in $\bar{\lambda}_f$. This is more clearly illustrated in Fig. 6, which shows the respective TBDLT parameter ϑ as a function of the sample temperature. The closed symbols are the experimental data while the open symbols were obtained from modeling calculations described in detail elsewhere [12]. The temperatures at which laser-induced cooling and heating are exactly balanced, T_{ZCT} , are found by interpolation to be 238 and 158 K for Samples 4 (filled circles) and 7 (filled squares), respectively. Note that ϑ goes through a maximum around 133 K for Sample 7. With decreasing temperature, the pump absorption coefficient decreases and causes the sample to heat less, while the cooling efficiency decreases

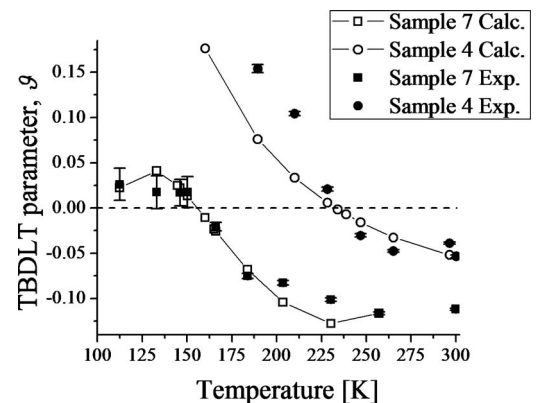


Fig. 6. TBDLT parameter as a function of ambient temperature for Samples 4 (circles) and 7 (squares). Open symbols indicate ϑ calculated from a theoretical model [12], while closed symbols indicate experimental data. Points below the horizontal line ($\vartheta < 0$) indicate laser-induced cooling while points above the line ($\vartheta > 0$) indicate heating. From this data, the T_{ZCT} can be deduced as 238 K for Sample 4 and 158 K for Sample 7.

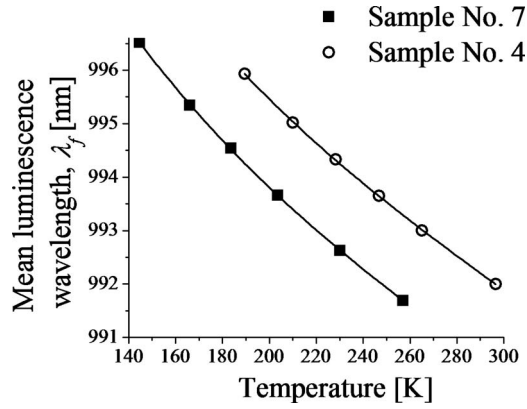


Fig. 7. Mean luminescence wavelength $\bar{\lambda}_f(T)$ as a function of temperature for Samples 4 (open circles) and 7 (filled squares). The cubic polynomial fits (solid lines) were used to interpolate $\bar{\lambda}_f(T)$ at temperatures of interest. The mean luminescence wavelength is defined as $\bar{\lambda}_f(T) = \int \lambda I(\lambda, T) d\lambda / \int I(\lambda, T) d\lambda$ which is calculated from luminescence spectra $I(\lambda, T)$.

and causes the sample to heat more. The maximum at 133 K is a result of these two competing effects.

The 150 K measurement of ϑ for Sample 7 has an uncertainty that is just above the zero line, indicating that this temperature change is just resolvable with the TBDLT technique. The calculated laser-induced temperature change at this point is ~ 7 mK [12], a value that is representative of the sensitivity of the TBDLT method. This sensitivity is indicative of what can be achieved for a Yb^{3+} -doped ZBLAN glass. Other materials will have different luminescence spectra with different temperature dependences and may thus lead to a different sensitivity.

Figure 7 shows the mean luminescence wavelength $\bar{\lambda}_f(T)$ calculated from the luminescence spectra recorded at different temperatures for Samples 4 and 7. $\bar{\lambda}_f(T)$ is fit with a cubic polynomial function, and the respective fits (solid lines in Fig. 7) can be used to calculate $\bar{\lambda}_f(T_{ZCT})$. Using T_{ZCT} found in Fig. 6, this yields 993.9 ± 0.4 and 995.9 ± 0.4 nm for Samples 4 and 7, respectively. Given the fixed laser wavelength of 1020.6 nm, the net quantum efficiency $\eta = \bar{\lambda}_f / \lambda_p$ can now be calculated to yield $(97.39 \pm 0.01)\%$ (at 238 K) and $(97.58 \pm 0.01)\%$ (at 158 K) for Samples 4 and 7, respectively. The higher T_{ZCT} and slightly lower net quantum efficiency of Sample 4 indicate that this sample had a higher concentration of impurities than the commercial Sample 7, demonstrating that pre-

cise measurements of net quantum efficiency efficiencies are possible with the TBDLT. These values are also summarized in Table 2.

A more detailed discussion of the net quantum efficiency in Eq. (4) is instructive, as past reports of the quantum efficiency were higher than those we report here [13]. This lower η in the present experiments is due to the fact that the material is pumped at a longer wavelength where the absorption efficiency [η_a , in Eq. (5)] is lower, indicating the presence of impurities. In an impurity-free material, $\alpha_b = 0$ and $\eta \sim \eta_{\text{ext}}$. As shown in Table 2, this is clearly not the case for Samples 4 and 7. Given η_{ext} and $\alpha_r(T_{ZCT}, \lambda_p)$, α_b can be calculated. Background absorption coefficients of $\alpha_b = 5.42 \times 10^{-4} \text{ cm}^{-1}$ and $\alpha_b = 3.11 \times 10^{-4} \text{ cm}^{-1}$ are found for Samples 4 and 7, respectively, indicating a lower impurity concentration in Sample 7. This trend is in agreement with a lower T_{ZCT} for Sample 7, compared to Sample 4.

An even more expeditious characterization can be done by simply measuring the TBDLT parameter ϑ at room temperature. As seen in Fig. 6, a smaller value of ϑ corresponds to a lower T_{ZCT} and thus a higher quantum efficiency. While a room-temperature measurement alone does not provide T_{ZCT} or η , it allows for a relative comparison of the performance of different laser-cooling samples. All samples listed in Table 1 were characterized in this manner, and the respective ϑ values are shown in Fig. 8. Sample 1 clearly illustrates that even the best commercial metal fluorides have insufficient purity to enable laser cooling; this sample showed substantial laser-induced heating even at room temperature. Purification of precursor materials along with a sufficiently high InF_3 oxidizer concentration, optimized hydrogen fluoride drying, and sufficiently long melting times provide a substantial improvement of laser-cooling performance as evident from the successive implementation of these processes in Samples 2–4. The 1% Yb^{3+} concentration of Sample 4 was increased to 2% in Sample 5, which resulted in substantial heating. The rate of energy migration among Yb^{3+} ions increases with increasing Yb^{3+} concentration, and some of the excitations can find impurity sites where non-radiative relaxation takes place. This process is more efficient in the 2% sample (Sample 5) compared to the 1% sample (Sample 4), and the fact that Sample 5 showed substantial heating is direct evidence for energy migration to transition-metal and/or OH^- impurity sites. Also note that the use of ZrF_4 purified by sublimation (Sample 6) resulted in a sample that cooled, however not as much

Table 2. Summary of Parameters Critical for Assessment and Comparison of Samples 4 and 7. T_{ZCT} and η were Measured as Described in Detail in this Article. η_{ext} was Measured Using a Thermal Camera and a Ti:Sapphire Pump Source in a Fractional Heating Experiment as Described Elsewhere [14]. η_{abs} was Derived from the Measurements of η and η_{ext} . α_b was Calculated Given η_{abs} and α_r . Sample 7 has lower T_{ZCT} , η_{abs} , α_b , and higher η and η_{ext} , Indicating That It Contained Fewer Impurities as Compared to Sample 4. The Values for η_{abs} , α_b , and α_r are Reported at T_{ZCT} and $\lambda_p = 1020.6$ nm

	T_{ZCT} (K)	η_{ext}	η_{abs}	η	α_r (cm^{-1})	α_b (cm^{-1})
Sample 4	238	0.9906	0.9831	0.9739	0.0315	5.42×10^{-4}
Sample 7	158	0.9942	0.9815	0.9758	0.0165	3.11×10^{-4}

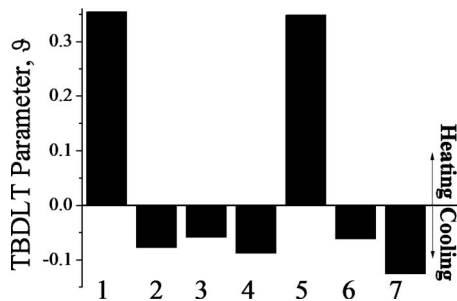


Fig. 8. TBDLT parameter ϑ [measured in vacuum at room temperature ($T=296$ K) and with $\lambda_p=1020.5$ nm] for a qualitative comparison of several ZBLANI:Yb³⁺ samples fabricated in our laboratory (Samples 1–6) and one sample commercially procured (IPG, Sample 7). A positive ϑ corresponds to heating, while a negative ϑ corresponds to local laser-induced cooling. Here we show a steady improvement in our purified materials over those produced with commercially available starting materials.

as the best sample fabricated from precursors purified by solvent extraction.

5. CONCLUSIONS

We have successfully demonstrated the TBDLT—a non-contact spectroscopic technique for measuring laser-induced temperature changes in optical materials. This method was used to characterize and benchmark the performance of optical refrigerator materials. The TBDLT method uses two commercially available bandpass filters to select regions of the luminescence spectra that show different temperature dependences. These temperature-induced luminescence intensity changes can quantify laser-induced heating and cooling processes. The TBDLT achieved a sensitivity of 7 mK and could successfully detect the temperature at which laser-induced heating and cooling are exactly balanced. We have shown that the net quantum efficiency can be obtained with a high precision using the TBDLT. Several Yb³⁺-doped fluorozirconate glasses were characterized by this method, and the results provided valuable feedback to the development of material purification and fabrication processes. The best ZBLANI:1% Yb³⁺ sample produced in our laboratory had a T_{ZCT} of 238 K and a corresponding net quantum efficiency of 97.39% at a pump wavelength of 1020.6 nm. This laser-cooling performance is a substantial improvement over samples prepared from commercial-grade high-purity metal fluoride precursors. While the TBDLT technique was shown to be an expedient and effective experimental method for characterizing the laser-cooling performance of Yb³⁺-doped fluorozirconate glasses, it can be adapted easily to other rare-earth-doped crystals and glasses. The TBDLT enables a key diagnostic capability that is critical to the further development of high-performance solid-state optical cryocoolers.

ACKNOWLEDGMENTS

We thank Dr. Scott R. Greenfield, Los Alamos National Laboratory (LANL), for useful discussions on the DLT. We

thank Dr. Karl Krämer at the Department of Chemistry and Biochemistry, University of Bern, Switzerland, for his assistance with the hydrogen fluoride gas drying apparatus used in the synthesis of the ZBLANI samples and for providing the sublimated ZrF₄ used for the synthesis of sample 6. We gratefully acknowledge the support of the U.S. Air Force Office of Scientific Research (AFOSR) under the Multidisciplinary University Research Initiative (MURI) program and the U.S. Department of Energy (DOE) through the LANL/Laboratory Directed Research and Development Program for this work. Los Alamos National Laboratory, an affirmative action equal opportunity employer, is operated by Los Alamos National Security, LLC, for the National Nuclear Security Administration of the U.S. DOE under contract DE-AC52-06NA25396.

REFERENCES

1. R. I. Epstein, M. I. Buchwald, B. C. Edwards, T. R. Gosnell, and C. E. Mungan, "Observation of laser-induced fluorescent cooling of a solid," *Nature* **377**, 500–503 (1995).
2. M. P. Hehlen, in *Optical Refrigeration: Science and Applications of Laser Cooling of Solids*, R. I. Epstein and M. Sheik-Bahae, eds. (Wiley, 2009), pp. 33–68.
3. W. M. Patterson, M. P. Hehlen, R. I. Epstein, and M. Sheik-Bahae, "Synthesis and evaluation of ultra-pure rare-earth-doped glass for laser refrigeration," *Proc. SPIE* **7228**, 72280C (2008).
4. D. Seletskiy, M. P. Hasselbeck, M. Sheik-Bahae, R. I. Epstein, S. Bigotta, and M. Tonelli, "Cooling of Yb:YLF using cavity enhanced resonant absorption," *Proc. SPIE* **6907**, 69070B (2008).
5. D. V. Seletskiy, S. D. Melgaard, S. Bigotta, A. Di Lieto, M. Tonelli, R. I. Epstein, and M. Sheik-Bahae, "Demonstration of an optical cryocooler," in *Conference on Lasers and Electro-Optics/International Quantum Electronics Conference*, OSA Technical Digest (CD) (Optical Society of America, 2009), paper IPDA9.
6. R. Frey, F. Micheron, and J. P. Pocholle, "Comparison of Peltier and anti-Stokes optical coolings," *J. Appl. Phys.* **87**, 4489–4498 (2000).
7. G. Mills and A. Mord, "Performance modeling of optical refrigeration," *Cryogenics* **46**, 176–182 (2006).
8. G. Lamouche, P. Lavallard, R. Suris, and R. Grousseau, "Low temperature laser cooling with a rare earth doped glass," *J. Appl. Phys.* **84**, 509–516 (1998).
9. V. K. Rai, "Temperature sensors and optical sensors," *Appl. Phys. B* **88**, 297–303 (2007).
10. B. Imangholi, M. P. Hasselbeck, D. A. Bender, C. Wang, M. Sheik-Bahae, R. I. Epstein, and S. Kurtz, "Differential luminescence thermometry in semiconductor laser cooling," *Proc. SPIE* **6115**, 215–220 (2006).
11. D. V. Seletskiy, M. P. Hasselbeck, M. Sheik-Bahae, and R. I. Epstein, "Fast differential luminescence thermometry," *Proc. SPIE* **7228**, 72280K (2009).
12. W. M. Patterson, M. Sheik-Bahae, R. I. Epstein, and M. P. Hehlen, "Model of laser-induced temperature changes in solid-state optical refrigerators," *J. Appl. Phys.* (to be published).
13. M. Sheik-Bahae and R. I. Epstein, "Optical refrigeration," *Nat. Photonics* **1**, 693–699 (2007).
14. M. P. Hehlen, R. I. Epstein, and H. Inoue, "Model of laser cooling in the Yb³⁺-doped fluorozirconate glass ZBLAN," *Phys. Rev. B* **75**, 144302 (2007).